



Highly selective production of value-added γ -valerolactone from biomass-derived levulinic acid using the robust Pd nanoparticles

Kai Yan ^{a,*}, Todd Lafleur ^a, Guosheng Wu ^a, Jiayou Liao ^b, Chen Ceng ^a, Xianmei Xie ^c

^a Department of Chemistry, Lakehead University, 955 Oliver Road, Thunder Bay, ON P7B 5E1, Canada

^b School of Chemical Engineering and Technology, Tianjin University, 92 Weijin Road, Tianjin 300072, China

^c College of Chemical Engineering, Taiyuan University of Technology, 79 Yingze Street, Taiyuan 030024, China



ARTICLE INFO

Article history:

Received 23 May 2013

Received in revised form 14 August 2013

Accepted 19 August 2013

Available online 28 August 2013

Keywords:

Synthesis

Pd Nanoparticle

Hydrogenation

Levulinic acid

γ -Valerolactone

ABSTRACT

A series of Pd nanoparticles deposited on the SiO₂ support were facilely and successfully synthesized in the presence of the green solvent CO₂, where the uniform distribution of Pd with small particle size was successfully achieved. The resulting Pd/SiO₂ nanoparticles catalysts exhibited excellent catalytic performances in the selective hydrogenation of biomass-derived levulinic acid, showing close to perfect selectivity of biofuel γ -valerolactone with the TON of 884.7 at 97.3% conversion of levulinic acid. The catalytic performance was superior to the activities of the 5 wt% Pd/SiO₂ nanoparticle catalyst prepared by the traditional impregnation method. Besides, the reaction parameters (e.g., the Pd loading, reaction time, reaction temperature, and hydrogen pressure), catalyst stability and reaction mechanism on the hydrogenation performance were studied. The resulting Pd nanoparticles catalysts behaved high stability in the hydrogenation.

© 2013 Elsevier B.V. All rights reserved.

1. Introduction

Currently, environmental protection and efficient use of natural resources are the sustainable alternatives to transform our society into a greener future [1–3]. The utilization of biomass or biomass-derived products is becoming vitally crucial, because it is aimed not only at the development of effective and environmentally benign technology, but also simultaneously solves the problem of agricultural and forestry waste use [4,5]. In most of the approaches being investigated, platform chemical levulinic acid (LA) has often been hydrogenated to produce value-added chemicals and biofuels [6–8], which is produced from the renewable cellulose [8,9]. A family of valuable chemicals (e.g., γ -valerolactone (GVL), pentanoic acid) and attractive biofuels (e.g., 2-methyltetrahydrofuran (2MTHF) and GVL) can be produced from LA as shown in Scheme 1 [10–12]. It was recently proposed that GVL, a frequently used food additive, exhibits the most important characteristics of an ideal liquid for the sustainable production of energy and carbon-based products [13]. It is renewable, has low melting point of -31°C , high boiling point of 207°C and flash point of 96°C , a definitive but acceptable smell for easy recognition of leaks and spills, low toxicity, and high solubility in water to assist biodegradation [13]. Besides, Horvath et al. [13,14] have shown that GVL does not

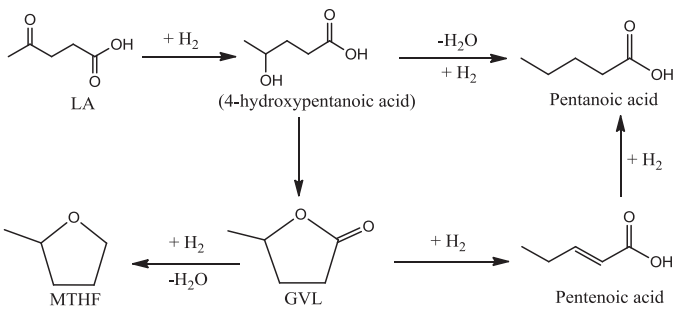
hydrolyze under neutral conditions, making it a safe material for large scale use. A comparative evaluation performed on a mixture of 10 v/v% GVL or EtOH and 90 v/v% 95-octane gasoline, show very similar properties [15].

The production of GVL was often obtained by the hydrogenation of LA through the reaction C₅H₈O₃ + H₂ \rightarrow C₅H₈O₂ + H₂O (pathway 1). However, to exert the hydrogenation of LA efficiently into GVL, its undesired side reaction to MTHF via the reaction C₅H₈O₂ + 2H₂ \rightarrow C₅H₁₀O + H₂O (pathway 2) must be avoided. Studies have shown that a critical dependency of the hydrogenation of LA via pathway 1, avoiding of the side reaction of GVL via pathway 2, depended on the catalyst and the catalytic reaction system [10,12].

Recent studies have shown that LA could be transformed into GVL (pathway 1) using the Ru-based homogeneous catalyst system [10,16,17]. High conversion of LA as well as good selectivity of GVL has been reported. However, the recycle and separation of the homogeneous catalyst from reaction residues later on was still a challenge. Subsequently, more attractive heterogeneous catalyst was developed due to its easy recycle. The most often employed catalysts were on the Ru-based nanocatalysts [18,19]. Manzer reported that 97% yield of GVL was obtained using Ru/C catalyst at 150°C and 34.5 bar H₂ in dioxane solvent [18]. Bourne et al. [19] reported that 99% yield of GVL was achieved using the Ru/Al₂O₃ catalyst under 200°C and 20 MPa H₂ via water in combination with supercritical CO₂ as the reaction medium. The inherent drawback existed in the utilization of Ru-catalysts was the stability and

* Corresponding author. Tel.: +1 807 627 3059.

E-mail addresses: kyan@lakeheadu.ca, xmsxty@sina.com (K. Yan).



Scheme 1. Hydrogenation of LA to value-added chemicals and biofuels.

deactivation [20]. More recently, our previous studies have shown that the Cu-based catalysts derived from their hydrotalcite precursors were efficient for the hydrogenation of LA. However, the Cu-catalysts were fabricated through several steps and required the regeneration [21,22]. The development of a more stable solid catalyst with high performance remains challenging.

Considering the aforementioned challenges for the production of biofuel GVL from biomass-derived LA, we conceived of a series of more stable and robust Pd nanoparticles (Pd/SiO_2) catalysts that were facilely fabricated by the assistance of green solvent CO_2 . The approach developed in this work avoids the use of aqueous means, allows the minimization of liquid waste generation, improves rapid separation of products [23,24], thus, can be considered as facile and eco-friendly approach. The resulting Pd nanoparticles catalysts presented uniform distribution with small particle size, and exhibited excellent performances in the hydrogenation of biomass-derived LA, showing close to perfect selectivity of GVL with the TON of 884.7 at 97.3% conversion under mild conditions. The catalytic performance was superior to the values of the 5 wt% Pd/SiO_2 catalyst prepared by the traditional impregnation method. Consequently, the metal Pd loading, reaction temperature, hydrogen pressure, reaction time, catalyst stability and reaction mechanism were also studied in this work.

2. Experimental

2.1. Chemicals

SiO_2 (surface-area of $220 \text{ m}^2/\text{g}$), palladium (II) acetate ($\text{Pd}(\text{OAc})_2$, $\geq 99.9\%$ trace metals basis), levulinic acid (98%), pentanoic acid ($\geq 99\%$), 1,4-pentanediol (99%), γ -valerolactone (99%), 2-methyltetrahydrofuran (analytical standard) were bought from Sigma-Aldrich. Pure H_2O was obtained from a NANOpure[®] Diamond TM UV ultrapure water purification system. All the chemicals were directly used without further treatment after purchase.

2.2. Catalyst preparation

A series of Pd nanoparticles were prepared using the Pd precursor ($\text{Pd}(\text{OAc})_2$) deposited on the amorphous SiO_2 support, which was prepared in the presence of CO_2 similarly reported as previous studies [25,26]. The general procedure was described in Fig. S1 and the typical procedure was performed as following: firstly, a constant amount of SiO_2 support ($\sim 0.3 \text{ g}$) and the precalculated amount of $\text{Pd}(\text{OAc})_2$ was added into a 50 mL micro-vessel. After this, the vessel was sealed and filled with $\sim 18 \text{ g}$ CO_2 . The vessel was under the stirring condition for another 24 h to ensure the high dispersion of the $\text{Pd}(\text{OAc})_2$ at room temperature. After this step the vessel was depressurized and the sample was calcined at 450°C for 6 h in the oven with air environment, whereby organic compounds were burned and removed. Finally, the

sample was pressurized with liquid CO_2 and reduced with H_2 at room temperature for 12 h under the stirring condition.

In comparison, 5 wt% Pd/SiO_2 nanoparticle was prepared by the traditional impregnation method in the liquid solution. The typical procedure was performed as following [20,27]: firstly, the pre-calculated amount of $\text{Pd}(\text{OAc})_2$ was added into 5 mL H_2O , then impregnated with the SiO_2 support ($\sim 0.3 \text{ g}$) for 24 h. After this, the solvent H_2O was slowly evaporated under 110°C and then calcinated at 450°C for 6 h in the furnace with air environment. Finally, the sample was reduced by H_2-N_2 (v/v ratio of 10/90) at 200°C for 3 h.

2.3. Characterizations

The resulting nanoparticles catalysts were examined by transmission electron microscopy (TEM) to investigate structural features with a JEOL-2010 instrument. The mean particle size d was calculated from the following formula: $d = \sum n_i d_i / \sum n_i$, where n_i is the number of particles of size d_i . The detection limit is about 1 nm for the supported Pd particles. The energy-dispersion X-ray (EDX, Hitachi SU-70) mapping was further employed to verify the existence and dispersion of elements in the resultant samples. The powder X-ray diffraction (XRD) patterns for the crystal phase analysis were collected on a Bruker AXS D8 Advance with $\text{Cu K}\alpha_1$ of 1.54060 \AA as a radiation source. The data were collected in the range of 25° to 90° with intervals of 0.05° and the scanning rate of $10^\circ/\text{min}$. The particle size for each sample has been calculated from the Scherrer equation (1), where λ corresponds to the $\text{Cu K}\alpha$ radiation, and β is the full width at half-maximum for a reflection maximum located at 2θ .

$$L = \frac{0.9\lambda}{\beta \cos \theta} \quad (1)$$

X-ray photoelectron spectroscopy (XPS) measurements were performed with an ESCALAB 250 spectrometer with a hemispherical analyzer and a monochromatized $\text{Al K}\alpha$ X-ray source ($E = 1486.6 \text{ eV}$), operated at 15 kV and 15 mA . For the narrow scans, analyzer pass energy of 40 eV was applied. The temperature-programmed reduction was carried out in a U-shaped quartz reactor placed in a furnace controlled by a temperature programmer (Omega Model CN 2000).

The reducibility of the calcined samples was determined by H_2 -temperature-programmed reduction (TPR). In these measurements, 50 mg of a sample was placed in a quartz reactor and heated at $10^\circ\text{C}/\text{min}$ up to 550°C under a He flow of $20 \text{ mL}/\text{min}$, and held at this temperature for 1 h. The reactor was then cooled down to 0°C and the sample exposed to a stream of $5\% \text{ H}_2/\text{Ar}$ at a flow rate of $20 \text{ mL}/\text{min}$. Subsequently, the sample was heated up to 400°C at a heating rate of $10^\circ\text{C}/\text{min}$. The amount of hydrogen consumed as a function of temperature was monitored on-line on a TCD detector. The maximum rate of H_2 consumption was used to choose the reduction temperature for each catalyst to be conducted in situ before reaction.

2.4. Hydrogenation of LA

The hydrogenation of LA was performed in a 25 mL micro-vessel (Parr Company) with the external temperature controller and pressure indicator. Typically, LA ($\sim 5.0 \text{ g}$) was dissolved in deionized water (5 mL) and then transferred into the vessel. After this, the catalyst ($\sim 0.1 \text{ g}$) was added, followed by the repeated procedure of filling argon and slowly making vacuum for three times. After reactions, the vessel was cooled down by water. The reaction products were firstly centrifuged for 30 min and then filtrated to obtain clear solution. The samples were analysed by GC (Shimadzu 2014, Column: 30 m DBWaxetr, FID Detector; the

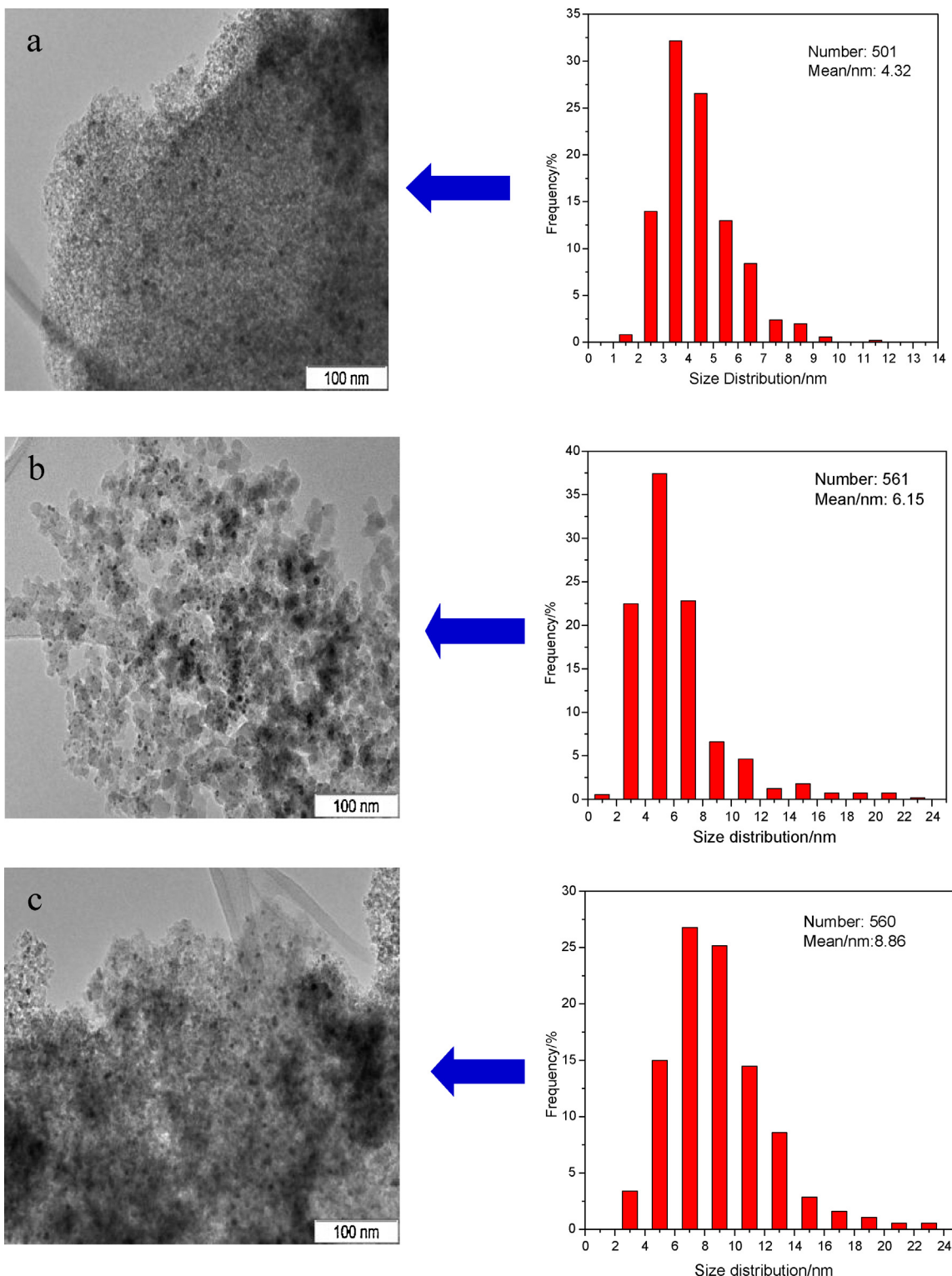


Fig. 1. TEM images of the resulting Pd/SiO₂ nanoparticles catalysts: (a) 3 wt%, (b) 5 wt%, (c) 7 wt%.

column temperature was raised from 40 to 250 °C with a heating rate of 3 °C/min; the injector temperature was set at 350 °C with a heating speed of 10 °C/min and the sampling volume was 0.2 μL). The potential Pd leach was detected by inductively coupled plasma-mass spectroscopy (ICP-MS, Perkin-Elmer Elan DRC-e).

3. Results and discussion

3.1. Characterizations of catalysts

Fig. 1 shows the representative TEM images of the as-prepared Pd/SiO₂ nanoparticles catalysts. TEM images (Fig. 1) revealed

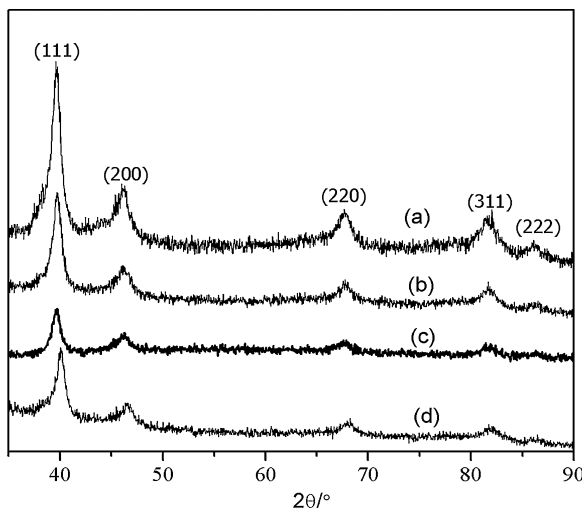


Fig. 2. Powder X-ray diffraction patterns of the resulting Pd/SiO₂ nanoparticles catalysts: (a) 3 wt%, (b) 5 wt%, (c) 7 wt%, (d) 5 wt% prepared by the traditional impregnation method.

that uniform and small Pd nanoparticles were homogeneously dispersed on the amorphous SiO₂ support. TEM measurement indicated that the mean size of Pd nanoparticle was 4.32 nm in the case of 3 wt% loading. With the Pd loading increasing to 5 wt%, more black dots of Pd nanoparticles were observed and the mean particle size was 6.15 nm. Further increasing the Pd loading to 7 wt% (Fig. 1c), the bigger size of Pd with a mean particle size of 8.86 nm was observed.

EDX analysis was used to further confirm the existence of Pd and the element distribution in the resulting samples, EDX mapping of the representative 5 wt% Pd/SiO₂ nanoparticle catalyst is shown in Fig. S2. Highly homogeneous dispersion of Pd, Si, O in the 5 wt% Pd/SiO₂ nanoparticle catalyst was observed (Fig. S2). Besides, no distinct difference of Pd amount was revealed by the EDX analysis in several different areas, indicating the uniform dispersion of Pd nanoparticles in the sample.

The amorphous SiO₂ support and the synthesized nanoparticles catalysts are further studied by XRD tests (Fig. S3 and Fig. 2). The peak at ~22° in Fig. S3 indicated the amorphous silica. The diffraction peaks (Fig. 2) indexed as 2θ of (111) approximately at 40.1°, (200) at 46.3°, (220) at 67.7°, (311) at 81.8°, and (222) at 86.5°, were identified as a single fcc phase of palladium [28]. The experimental pattern matched well with the standard crystal graph (JCPDS PDF 01-087-0643, Fm-3m, $a=b=c=0.3908\text{ nm}$) for the syn-Pd⁰. Besides, no other phase (e.g. PdO) was observed, which confirmed that the bulk Pd/SiO₂ nanoparticles catalysts were successfully reduced. For the 1 wt% Pd loading, the diffraction peaks were too weak, which was possibly due to the detection limit of the XRD fixture. With the Pd loading increasing (Fig. 2a–c), the peaks appeared more intense. Furthermore, the crystal size of 4.5 nm, 6.7 nm and 9.0 nm was calculated based on the Scherrer Equation, respectively, which was close to the mean size measured by TEM images (Fig. 1). In comparison, the 5 wt% Pd/SiO₂ catalyst prepared by the traditional impregnation method was also successfully reduced as shown in the XRD pattern (Fig. 2d).

For the supported metal nanoparticles, the metal surface was easy to be oxidized during the preparation process due to the unstable thermodynamic property of Pd⁰. A different chemical environment of the atoms at the interface will generally lead to the appearance of new spectral features in the XPS spectra. Thus XPS was employed and the recorded XPS patterns of the representative 3 wt%, 5 wt% and 7 wt% Pd/SiO₂ nanoparticle catalysts are shown in Fig. S4. The presence of two prominent sets of Pd (3d) peaks,

Table 1

Catalytic activities of the resulting Pd/SiO₂ nanoparticles catalysts in the hydrogenation of LA.^a

No.	Catalyst	Conv. (LA)/%	Sel. (GVL)/%	TON ^b
1	1 wt% Pd/SiO ₂	8.6	95.2	375.1
2	3 wt% Pd/SiO ₂	30.2	99.1	457.2
3	5 wt% Pd/SiO ₂	57.3	98.9	519.4
4	7 wt% Pd/SiO ₂	75.6	97.8	484.0
5 ^b	5 wt% Pd/SiO ₂	32.8	90.7	272.7

^a Hydrogenation conditions: m(LA)=5.0 g, m(catalyst)=0.10 g, V(H₂O)=5 mL, p(H₂)=50 bar, T=160°C, t=6 h, stirring speed = 1000 rpm. [b] Catalyst was prepared by the impregnation method as described in Experimental section.

^b Turnover numbers (TON)=the molar of the GVL/the molar of the metal catalyst used.

corresponding to the 3d_{3/2} and 3d_{5/2} orbital states. The peak regions of Pd can be fitted with two sets of peaks at 340.6 eV (3d_{3/2}) and 335.3 eV (3d_{5/2}), which indicated that the successful reduction was achieved. Besides, the very weak peak was observed at 341.7 eV and 336.5 eV, which was possible due to the presence of very small amount of PdO on the surface or the interaction between of Pd and the oxygen from the SiO₂ support [29].

The TPR profiles of the chosen 3% Pd/SiO₂ and 5% Pd/SiO₂ catalysts are compared in Fig. S5. For 3% Pd/SiO₂ catalyst, the TPR profile mainly exhibits one peak centered on ~105°C, indicative of the H₂ consumption [30]. The H₂ profile was consistent with the decomposition of Pd(OAc)₂, which was reported to form at room temperature over large Pd particles (>2 nm) [31]. The other weak peak at ~150°C, was ascribed to water evolution as previously reported in [32,33]. In the case of 5 wt% Pd/SiO₂, the main peak was observed at ~125°C, which was from the reduction of Pd(II) to Pd(0). It is also worth noting that the higher amount of Pd decreases the reducibility of Pd, leading to a shift toward a little higher temperatures, which indicated that bigger particle size was existed. Besides, a second broader peak was detected in the range of 200–350°C, which was due to the water evolution [32,33].

3.2. Hydrogenation of LA to GVL

3.2.1. Influence of Pd loading

Table 1 reports the catalytic results obtained for the resulting Pd/SiO₂ nanoparticles catalysts in the hydrogenation of biomass-derived LA. It was interesting to find that high selectivity of GVL was achieved in the presence of Pd/SiO₂ nanoparticles catalysts. The metal Pd loading presented crucial influence on the observed

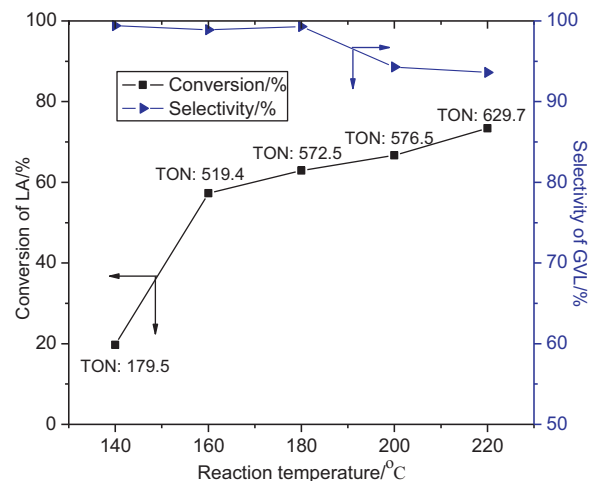


Fig. 3. Influence of reaction temperature on the catalytic activities. Note: Hydrogenation conditions: m(LA)=5.0 g, m(catalyst)=0.1 g, V(H₂O)=5 mL, p(H₂)=50 bar, t=6 h, stirring speed = 1000 rpm.

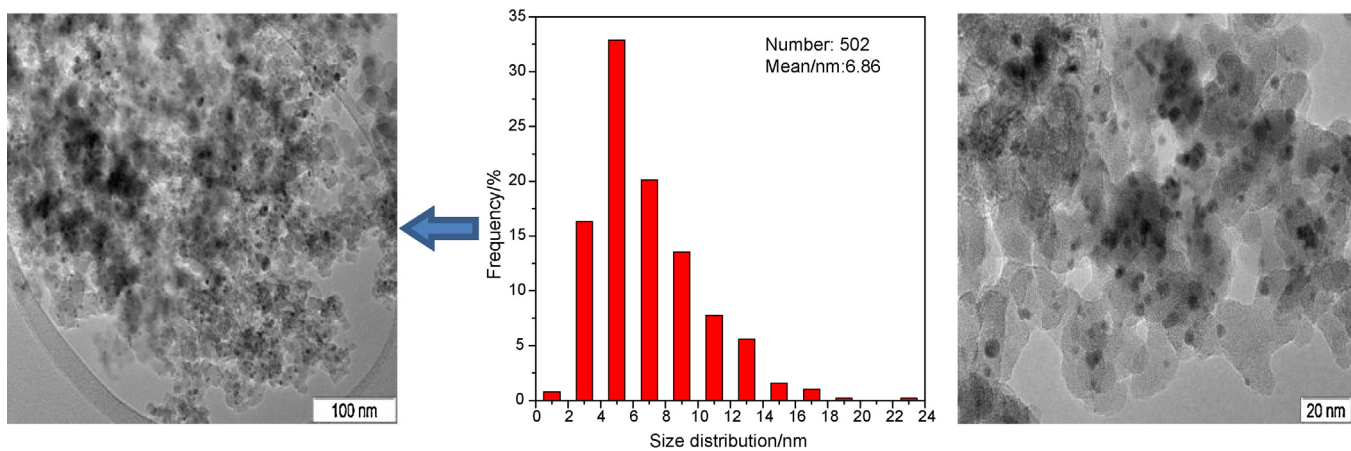


Fig. 4. TEM analysis of the reduced 5 wt% Pd/SiO₂ nanoparticles catalyst.

catalytic activities. With the Pd loading increasing from 1 wt% to 7 wt% (No. 1–4), the conversion of LA increased clearly from 8.6% to 75.6% and the TON value ranged between 375.1 and 519.4. These results indicated that Pd loading can be used to alter the extent of hydrogenation, where the uniform Pd with small size (Fig. 1) would play a role. Reviewing the catalytic performance in Table 1, 95.2% selectivity of GVL with the TON of 375.1 at the 8.6% conversion of LA was observed when the 1 wt% Pd/SiO₂ nanoparticles catalyst was employed (No. 1). While 98.9% selectivity of GVL with TON of 519.4 at 57.3% conversion of LA as well as was achieved in the case of 5 wt% Pd/SiO₂ nanoparticles catalyst (No. 3). In comparison, 5 wt% Pd/SiO₂ nanoparticles catalyst was prepared by the traditional impregnation method, displaying 90.7% selectivity with the TON of 272.7 at 32.8% conversion (No. 5). These results indicated that the crucial role of Pd in the hydrogenation. Based on the economic view and the catalytic performances (Table 1), 5 wt% Pd/SiO₂ nanoparticles catalyst was thus chosen for further studies.

3.2.2. Influence of reaction temperature

Fig. 3 reveals the reaction temperature influence on the catalytic activities. It was observed that the conversion of LA was increased from 19.7% to 73.4% and the TON ranged from 179.5 to 629.7 as the reaction temperature was raised from 140 to 220 °C. This was due to the fact that the high temperature would promote a faster reaction rate and mass transfer of reactants as well as H₂. However, too high temperature (e.g. 220 °C) would promote the side reactions and clearly decreased the selectivity of GVL. For example, 99.4% selectivity of GVL was achieved at 140 °C, which was reduced to 92.3% at 220 °C. Meantime, the GC detected the whole percentage of the side products (pentanoic acid and MTHF) were ~6.8% at 220 °C. Even at 200 °C, small amount (<5%) of pentanoic acid and MTHF was found, which indicated that side reactions would be more prone to occur at high temperature. Based on these results, 180 °C was thus chosen for further studies.

3.2.3. Influence of reaction time and hydrogen pressure

Table 2 presents the influence of reaction time and hydrogen pressure on the catalytic activities. The conversion of LA and the TON values increased with the prolonging reaction time (No. 1–4). At the reaction time of 4 h (No. 1), the conversion of LA was 39.4%, which was increased to 88.1% at the reaction time of 10 h (No. 4). However, further prolonging reaction time, it would cause the further ring-opening of GVL to pentanoic acid or MTHF, as detected by our GC and indicated by the decrease of the GVL selectivity (No. 1–4). The hydrogen pressure was subsequently studied at the reaction time of 6 h as shown in Table 2. As it turned out, the hydrogen pressure (No. 5–7) presented crucial influence on the conversion

of LA. The selectivity of GVL behaved relatively stable in general. High hydrogen pressure resulted in the rapid conversion of LA and higher TON values. For example, when 30 bar H₂ was employed (No. 5), 25.5% conversion of LA and the TON of 232.6 were achieved, where the conversion and TON were increased significantly to 97.3% and 884.7 under 90 bar H₂ (No. 7), respectively. This was possibly related to the fact that more H₂ was transported to the reactants, resulting a fast rate and higher conversion. Besides, to efficiently compare with the previous works, representative works from literatures [20–22,34–41] were summarized in Table S1. To our limited knowledge, our study shows the highest value obtained so far on the supported Pd catalysts. Even in comparison with the often utilized Ru-, Cu-, and Ir-catalysts, our results are still among the top-list as shown in Table S1 and the catalysts developed in this work are more selective for the production of GVL. Besides, the method to fabricate the metal catalyst developed in this work avoids the use of aqueous means, allows the minimization of liquid waste generation, improves a higher rate of mass transfer, and rapid separation of products, thus, can be considered as the simple, safe and ecofriendly route.

3.3. Recyclability tests

To understand the stirring speed on the catalytic performance, different stirring speed was tested as shown in Table S2. Increasing the stirring speed has very slide influence on the conversion and selectivity, which suggested that the mass transportation influence was weak. Subsequently, we focus on the recyclability tests of the resulting nanoparticle catalyst, the 5 wt% Pd/SiO₂ nanoparticle catalyst was recycled from reaction residues through centrifugation for 30 min, dried at 90 °C for 12 h, calcinated at 350 °C for 3 h and then reduced by H₂ in liquid CO₂. TEM is further employed to detect the potential aggregation of Pd nanoparticles in the process of reduction. TEM images and particle distribution are shown in

Table 2
Reaction time and hydrogen pressure on the catalytic activity.^a

Entry	Time/h	Pressure/bar	Conv. (LA)%	Sel. (GVL)%	TON
1	4	50	39.4	99.6	359.7
2	6	50	51.7	99.3	470.5
3	8	50	72.1	98.2	648.9
4	10	50	88.1	96.7	780.8
5	6	30	25.5	99.5	232.6
6	6	70	87.6	98.8	794.0
7	6	90	97.3	99.2	884.7

^a Other hydrogenation conditions: T = 180 °C, V(H₂O) = 5 mL, catalyst was 5 wt% Pd/SiO₂, m(catalyst) = 0.10 g, m(LA) = 5.0 g, stirring speed = 1000 rpm.

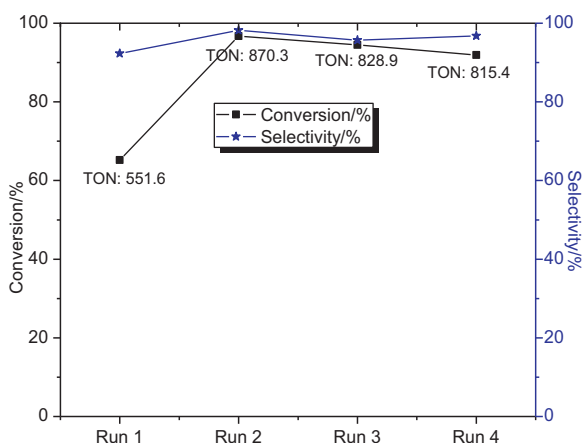


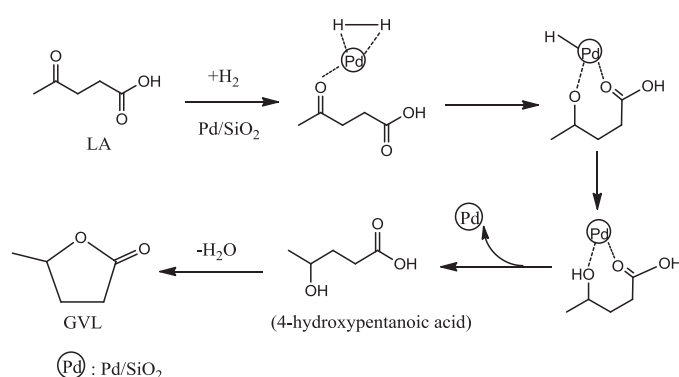
Fig. 5. Catalytic activities of the recycled 5 wt% Pd/SiO₂ nanoparticles catalyst. Note: Other conditions: $T=180^{\circ}\text{C}$, $V(\text{H}_2\text{O})=5\text{ mL}$, $t=6\text{ h}$, $p(\text{H}_2)=90\text{ bar}$, $m(\text{LA})=5.0\text{ g}$, $m(\text{catalyst})=0.10\text{ g}$, stirring speed = 1000 rpm.

Fig. 4. Uniform dispersion of Pd nanoparticles with a mean size of 6.86 nm was achieved (Fig. 4). No clear increase in the Pd nanoparticle size was found in comparison with the fresh 5 wt% Pd/SiO₂ nanoparticle catalyst.

The catalytic performances of the spent and reduced 5 wt% Pd/SiO₂ nanoparticles catalysts are shown in Fig. 5. When the spent 5 wt% Pd/SiO₂ nanoparticles catalyst was used for the hydrogenation of LA, 65.2% conversion was obtained with 92.3% selectivity of GVL and the TON of 551.6 (Run 1), which was a little lower than the values (99.2% selectivity and the TON of 884.7 at 97.3% conversion of LA) of the fresh 5 wt% Pd/SiO₂ nanoparticles catalyst, which was possible due to carbon deposit from the reactant and/or products [40]. Fortunately, the further hydrogenation using the reduced 5 wt% Pd/SiO₂ nanoparticles catalysts (Run 2–4), the selectivity of GVL behaved rather stable under the standardized conditions. Also the conversion of LA dropped slightly from 96.7% to 91.9% and the TON decreased from 870.3 to 815.4. These small decreases were most likely the result of an incomplete catalyst recovery in the procedure. Furthermore, analysis of the reaction solution after the third run revealed no detectable leach of Pd, which confirmed the high stability of Pd nanoparticles catalysts in this work.

3.4. Hydrogenation pathway of LA

Fig. S5 shows the representative GC spectrum of the products distribution in the hydrogenation of LA. Under the experimental conditions, a main reaction network for the formation of GVL was proposed in Scheme 2. It was proposed that the first step during the hydrogenation reaction was the chemisorption of molecular H₂



Scheme 2. Hydrogenation pathway of LA to GVL on Pd/SiO₂ nanoparticles catalysts.

and liquid LA [36,38], whereby the uniform dispersion of Pd⁰ with small size (Fig. 2) might play an important role. Molecular H₂ was adsorbed on the surface of Pd⁰ through the formation of hydrogen bonds between hydrogen with Pd. LA was also adsorbed on the surface of Pd in the combination of Pd⁰ with carboxylic C and O atoms [40,42]. When the first H was added to LA molecule, an intermediate that was linked by a σ -bond was formed. The intermediate was stabilized by its interaction with Pd⁰. If the intermediate acquired one more H atom, it then formed 4-hydroxypentanoic acid and further bonded on the metal surface. Then the hydroxyl group and the acid group would react to lose one molecule of water through the self-condensation, rapidly producing GVL [16,42].

4. Conclusions

A series of Pd nanoparticles supported on the SiO₂ support were successfully synthesized and exhibit efficient catalytic performance in the hydrogenation of biomass-derived LA, showing the perfect selectivity of biofuel GVL with high TON of 884.7 at 97.3% conversion of the 5 wt% Pd/SiO₂ catalyst under mild conditions of 180 °C, 6 h and 90 bar H₂. The facile, safe and eco-friendly approach to fabricate Pd nanoparticles in the presence of liquid CO₂, avoids the use of aqueous means, allows the minimization of liquid waste generation, and improves rapid separation of nanoparticles. The catalytic performance of the resulting Pd nanoparticles catalyst was superior to the values of the 5 wt% Pd/SiO₂ catalyst prepared by the traditional impregnation method. Besides, the parameters of Pd loading, reaction temperature and hydrogen pressure presented crucial influence on the catalytic performance.

Appendix A. Supplementary data

Supplementary data associated with this article can be found, in the online version, at <http://dx.doi.org/10.1016/j.apcata.2013.08.037>.

References

- [1] G.W. Huber, S. Iborra, A. Corma, Chem. Rev. 106 (2006) 4044–4098.
- [2] P.M. Mortensen, J.D. Grunwaldt, P.A. Jensen, K.G. Knudsen, A.D. Jensen, Appl. Catal. A 407 (2011) 1–19.
- [3] B. Kamim, Angew. Chem. Int. Ed. 46 (2007) 5056–5058.
- [4] J.J. Bozell, G.R. Petersen, Green Chem. 12 (2010) 539–554.
- [5] J.X. Xi, Y. Zhang, Q. Xia, X.H. Liu, J.W. Ren, G.Z. Lu, Y.Q. Wang, Appl. Catal. A 459 (2013) 52–58.
- [6] K. Yan, T. Lafleur, J.Y. Liao, J. Nanopart. Res. 15 (2013) 1906–1912.
- [7] D.M. Alonso, J.Q. Bond, J.A. Dumesic, Green Chem. 12 (2010) 1493–1513.
- [8] C.H. Zhou, X. Xia, C.X. Lin, D.S. Tong, J. Beltramini, Chem. Soc. Rev. 40 (2011) 5588–5617.
- [9] X.L. Tong, Y. Ma, Y.D. Li, Appl. Catal. A 385 (2010) 1–13.
- [10] F.M.A. Geilen, B. Engendahl, A. Harwardt, W. Marquardt, J. Klankermayer, W. Leitner, Angew. Chem. Int. Ed. 49 (2010) 5510–5514.
- [11] R. Luque, J.H. Clark, Catal. Commun. 11 (2010) 928–931.
- [12] D.M. Alonso, S.G. Wettstein, M.A. Mellmer, E.I. Gurbuz, J.A. Dumesic, Energy Environ. Sci. 6 (2013) 76–80.
- [13] I.T. Horvath, H. Mehdi, V. Fabos, L. Boda, L.T. Mika, Green Chem. 10 (2008) 238–242.
- [14] V. Fabos, G. Koczo, H. Mehdi, L. Boda, I.T. Horvath, Energy Environ. Sci. 2 (2009) 767–769.
- [15] K. Nasirzadeh, D. Zimin, R. Neuendorf, W. Kunz, J. Chem. Eng. Data 49 (2004) 607–612.
- [16] F.M.A. Geilen, B. Engendahl, M. Hölscher, J. Klankermayer, W. Leitner, J. Am. Chem. Soc. 133 (2011) 14349–14358.
- [17] H. Mehdi, V. Fábo, R. Tuba, A. Bodor, L.T. Mika, I.T. Horváth, Top. Catal. 48 (2008) 49–54.
- [18] L.E. Manzer, Appl. Catal. A 272 (2004) 249–256.
- [19] R.A. Bourne, J.G. Stevens, J. Ke, M. Poliakoff, Chem. Commun. (2007) 4632–4634.
- [20] S.G. Wettstein, J.Q. Bond, D.M. Alonso, H.N. Pham, A.K. Datye, J.A. Dumesic, Appl. Catal. B 117–118 (2012) 321–329.
- [21] K. Yan, J.Y. Liao, X. Wu, X.M. Xie, RSC Adv. 3 (2013) 3853–3856.
- [22] A.M. Hengne, C.V. Rode, Green Chem. 14 (2012) 1064–1072.
- [23] W. Leitner, Acc. Chem. Res. 35 (2002) 746–756.
- [24] C.H. Yen, K. Shimizu, Y.Y. Lin, F. Bailey, I.F. Cheng, C.M. Wai, Energy Fuels 21 (2007) 2268–2271.

- [25] J. Kim, G.W. Roberts, D.J. Kiserow, *Chem. Mater.* 18 (2006) 4710–4712.
- [26] J. Kim, M.J. Kelly, H.H. Lamb, G.W. Roberts, D.J. Kiserow, *J. Phys. Chem. C* 112 (2008) 10446–10452.
- [27] J. Wu, Y.M. Shen, C.H. Liu, H.B. Wang, C. Geng, Z.X. Zhang, *Catal. Commun.* 6 (2005) 633–637.
- [28] K. Yan, T. Lafleur, J.Y. Liao, X.M. Xie, *Sci. Adv. Mater.* 6 (2014) 1–6.
- [29] M. Flytzani-Stephanopoulos, B.C. Gates, *Annu. Rev. Chem. Biomol. Eng.* 3 (2012) 545–574.
- [30] A.F. Gusovius, T.C. Watling, R. Prins, *Appl. Catal. A* 188 (1999) 187.
- [31] J.J. Panpranot, O. Tangjittwattakorn, P. Praserthdam, J.G. Goodwin Jr., *Appl. Catal. A* 292 (2005) 322–327.
- [32] S. Fessi, A.S. Mamede, A. Ghorbel, A. Rives, *Catal. Commun.* 27 (2012) 109–113.
- [33] F. Sotoodeh, L. Zhao, K.J. Smith, *Appl. Catal. A* 362 (2009) 155–162.
- [34] Y. Gong, L. Lin, Z.P. Yan, *BioResources* 6 (2011) 686–699.
- [35] A.M.R. Galletti, C. Antonetti, V. De Luise, M. Martinelli, *Green Chem.* 14 (2012) 688–694.
- [36] P. Azadi, R. Carrasquillo-Flores, Y.J. Pagán-Torres, E.I. Gürbüz, R. Farnood, J.A. Dumesic, *Green Chem.* 14 (2012) 1573–1576.
- [37] X.L. Du, L. He, S. Zhao, Y.M. Liu, Y. Cao, H.Y. He, K.N. Fan, *Angew. Chem. Int. Ed.* 50 (2011) 7815–7819.
- [38] D.M. Alonso, S.G. Wetstein, J.Q. Bond, T.W. Root, J.A. Dumesic, *ChemSusChem* 4 (2011) 1078–1081.
- [39] P.P. Upare, J.M. Lee, D.W. Hwang, S.B. Halligudi, Y.K. Hwang, J.S. Chang, *J. Ind. Eng. Chem.* 17 (2011) 287–292.
- [40] Z.P. Yan, L. Lin, S. Liu, *Energy Fuels* 23 (2009) 3853–3858.
- [41] P.P. Upare, J.M. Lee, Y.K. Hwang, D.W. Hwang, J.H. Lee, S.B. Halligudi, J.S. Hwang, J.S. Chang, *ChemSusChem* 4 (2012) 1749–1752.
- [42] J.C. Serrano-Ruiz, D.J. Braden, R.M. West, J.A. Dumesic, *Appl. Catal. B* 100 (2010) 184–189.